7th European Workshop on Structural Health Monitoring
July 8-11, 2014. La Cité, Nantes, France

CRACK DETECTION IN MULTI-WIRE CABLES USING GUIDED ULTRASONIC WAVES

Christoph Schaal, Lothar Gaul

University of Stuttgart, Institute of Applied and Experimental Mechanics
Pfaffenwaldring 9, 70550, Stuttgart, Germany

schaal@iam.uni-stuttgart.de

ABSTRACT

Automated Structural Health Monitoring schemes are developed to cost-efficiently prevent failure of mechanical and civil structures, and to predict the structure's residual life. In this work, an efficient crack detection algorithm based on the Hilbert transform is presented. By means of this algorithm, crack localization in multi-wire cables is performed through a time-of-flight analysis of the wave packets. Crack identification can be performed by evaluating the waves' amplitudes. The algorithm is fully automatized and distinguishes between wave packets from different waves independently. Its applicability is analyzed for a single cylindrical wire and for multi-wire cables.

KEYWORDS : *Structural Health Monitoring, guided waves, damage diagnostics, signal processing, nonlinear waves*

INTRODUCTION

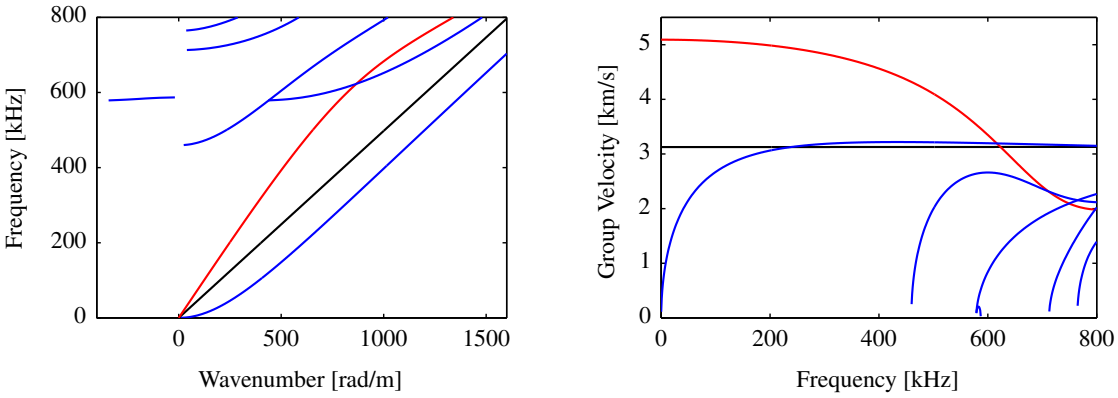
Mechanical and civil structures, such as overhead power lines and cables of suspension or cable-stayed bridges, have a finite life span. They deteriorate especially due to wind-induced vibrations, temperature changes and corrosion. Failure can lead to catastrophic collapse of these structures causing severe damage to people, the environment and the structure itself [1].

Active ultrasonic wave-based Structural Health Monitoring (SHM) schemes are developed to automatize damage detection. Guided waves are excited in the monitored multi-wire cables and are partially reflected at damages. Reflected waves are measured and damage detection algorithms determine whether or not defects exist. However, the multimodal and dispersive nature of wave propagation in cylindrical waveguides has to be accounted for [2]. Also, real cable structures do not consist of a single cylindrical wire but are composed of several coupled wires.

In order to evaluate the structural state, typically the following diagnostic levels are defined [3]: crack detection (level I), crack localization (level II), crack identification (level III) and prognosis of remaining lifetime (level IV). Using guided ultrasonic waves, a thorough crack analysis is possible. In addition to the detection of a crack, localization is achieved by a time-of-flight analysis. In combination with known wave speeds, the distance between the crack and the sensor is determined. Often such analyses are performed using the short time Fourier transform (STFT) or wavelet transform [4]. Moreover, crack identification, i.e. evaluating the severity of a damage, can be achieved. However, sophisticated simulations are required, including conventional finite element, boundary element, or hybrid methods [5, 6].

In this work, an efficient crack detection algorithm based on the Hilbert transform is presented, which can be implemented on low-cost wireless sensor nodes [7]. By means of this algorithm, levels I, II and III are achieved. The algorithm is fully automatized and distinguishes between wave packets from different waves independently. By a time-of-flight analysis of reflected wave packets, the position of the damage is determined via the wave speeds. The identification of, for example, the crack depth is achieved by a comparison with reference data from simulations. Its applicability is analyzed for a single cylindrical wire and for multi-wire cables, including comprehensive experimental studies.

Copyright © Inria (2014)



(a) $f(\mathrm{real}\,(k))$ (b) $c_\mathrm{g}(f)$

Figure 1: Dispersion curves for aluminum cylinders with radius $R = 2\,\mathrm{mm}$. Red lines represent longitudinal, blue lines flexural and black lines torsional modes, respectively

FUNDAMENTALS

Guided waves propagate in one direction while having characteristic spatial displacement fields (mode shapes) in all three axes. Solid bodies that allow for propagation of guided waves are called waveguides. The displacement fields $\underline{u}$ of guided waves in cylindrical structures can be written in the form

$$\underline{u}(\underline{x},t) = \underline{\hat{u}}(x,y)\,\mathrm{e}^{\mathrm{j}(kz-\omega t)} = \underline{\hat{u}}(r,\varphi)\,\mathrm{e}^{\mathrm{j}(kz-\omega t)}\,. \tag{1}$$

The waves are characterized by their respective mode shapes $\underline{\hat{u}}(r,\varphi)$ and propagate in z-direction with the angular frequency ω. Three types of waves may propagate in cylindrical waveguides: longitudinal, flexural and torsional waves [2]. Using common nomenclature, these waves are abbreviated as L(0,m), F(n,m) and T(0,m) with order n and sequential numbering m. For complex angular wavenumbers k, solutions with no imaginary part are considered as propagating waves, while solutions with a non-zero imaginary part are considered as non-propagating waves. Evanescent modes, which decay exponentially with distance, thereby form a subclass of non-propagating waves.

In order to localize cracks, wave propagation velocities must be known. With the angular wavenumber k and angular frequency ω, which are related by characteristic equations for each mode type, by definition the group velocity is

$$c_\mathrm{g} = \frac{\mathrm{d}\omega}{\mathrm{d}k}\,. \tag{2}$$

Instead of solving the analytical characteristic equations, displacement and traction fields as well as wavenumbers of propagating and non-propagating waves in waveguides are efficiently determined with the Waveguide Finite Element Method (WFEM) [8]. Thereby, only one thin section is considered in the FE modeling process. By solving the related eigenvalue problem for each frequency in the range of interest, dispersion curves are efficiently determined [9], as shown in Fig. 1. For the crack detection presented in the following, mainly the L(0,1) wave is used due to its superior properties. However, since mode conversion generally occurs at discontinuities, F(1,1) waves are also evaluated.

CRACK DETECTION ALGORITHM

In the following, a crack detection algorithm is presented, with which previously introduced diagnostic levels I, II and III for common SHM applications on multi-wire cables are accomplished. The algorithm is implemented as a three step procedure. Detecting reflected waves in the measured signal leads to diagnostic level I. Then, level II is achieved by a time of flight analysis for the detected wave

packets. Finally, diagnostics for level III are performed by a comparison of the waves' amplitudes with reference data from simulations.

Crack Detection and Localization

The goal of the crack detection and localization algorithm, presented in the following, is to automatically identify wave packets and detect reflections, which may arise from cracks and notches in cylindrical waveguides. By a time-of-flight analysis of reflected wave packets, the position of the damage is determined via the wave speeds. While often the STFT or wavelet transform are used for these tasks, in the following a method based on the Hilbert transform is presented. One major advantage of the Hilbert transform is that it can be efficiently implemented on low-cost wireless sensor nodes [7], allowing for a pre-evaluation of the structural state on the device and reducing the energy consumption for data transmission.

First, the analytic signal V_a is determined from the measured signal V_m using the Hilbert transformation, where the real part is the original data and the imaginary part is the Hilbert transform $V_\mathrm{H} = \mathscr{H}(V_\mathrm{m})$. The Hilbert-transformed sequence has the same amplitude and frequency content as the original real data and includes phase information that depends on the phase of the original data. Sines are transformed into cosines and vice versa. Hence, if the absolute value of the analytic signal is taken, i.e. $V_\mathrm{env} = |V_\mathrm{a}|$, then the envelope function V_env of the measured signal is derived. Note, V_m and therefore also V_H, V_a and V_env are functions of time. For brevity of notation, however, the arguments are omitted in the derivation when not necessary. Now, a threshold θ is defined according to the transducers' properties (e.g. amplitude of driving signal or sensor sensitivity). All levels above this threshold, i.e. $V_{\mathrm{env},i} > \theta$, are considered possible parts of propagating wave packets. Separation of these wave packets is achieved, when possible, using a comparison between the sampling time step and the time step between levels above the threshold. As dominant aspects of the N detected wave packets, the maximum $V_{\mathrm{max},i}$ for all time steps within a wave packet i is determined by

$$V_{\mathrm{max},i} = \max_t \left(V_{\mathrm{env},i}(t)\right) , \quad \text{for} \quad i = 1,\ldots,N \tag{3}$$

as well as the corresponding time $t_{\mathrm{max},i}$. Note, in the following, the index i is omitted for clarity. However, evaluations are still conducted for each wave packet individually. The wave packet's arrival time is calculated using the period T and the number of periods n_p of the incident wave. Regarding the incident wave packet used in this work, which is a Hann-windowed sinusoid, the start time t_S of the wave packet is given by

$$t_\mathrm{S} = t_\mathrm{max} - \frac{n_\mathrm{p}}{2} T \, . \tag{4}$$

Alternatively, the time t_S is decomposed into

$$t_\mathrm{S} = t_\mathrm{sens} + t_1 + t_2 \, , \tag{5}$$

where t_sens is the time the incident wave needs to travel from actuator to sensor, t_1 is the time from sensor to crack, and t_2 is the time of the reflected wave from crack to sensor (see Fig. 2). For an incident wave, both t_1 and t_2 must be zero. The paths 1 and 2, shown in Fig. 2, have the same length and are given by

$$d_1 = d_2 = z_\mathrm{crack} - z_\mathrm{sens} \, , \tag{6}$$

where z_crack is the position of the crack and z_sens is the position of the sensor. Note, without loss of generality, the position of the actuator z_act is assumed to be zero (see Fig. 2). Since an incident L(0,1) wave is assumed, the distance d_1 is given by $d_1 = c_{\mathrm{g,L}} t_1$. For an incident L(0,1) wave below the cut-off frequency of higher order modes, a reflected L(0,1) wave and an F(1,1) wave are scattered at the defect. Additionally occurring non-propagating waves are negligible here. Therefore, depending on

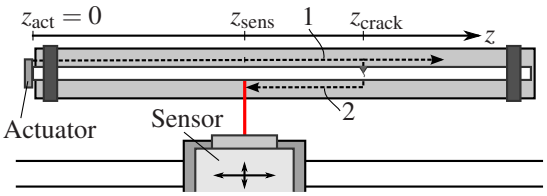


Figure 2: Guided wave analysis in the presence of a crack at z_{crack} using a piezoelectric actuator at $z = 0$ and measuring with an LDV at z_{sens}

the type of reflected wave, the distance d_2 is given by $d_2 = c_{g,L} t_2$ for a reflected L(0,1) wave, or by $d_2 = c_{g,F} t_2$ for a reflected F(1,1) wave, respectively. By solving Eq. (5) for t_2 and plugging the result along with previous relations into Eq. (6), the position of the crack is then determined by either

$$z_{crack,L} = z_{sens} + \frac{c_{g,L}}{2} (t_S - t_{sens}) \tag{7}$$

for a reflected L(0,1) wave, or by

$$z_{crack,LF} = z_{sens} + \frac{c_{g,L} c_{g,F}}{c_{g,L} + c_{g,F}} (t_S - t_{sens}) \tag{8}$$

for a reflected F(1,1) wave. In the first case, $t_2 = t_1$ holds since for both travel paths the wave speed is equivalent, whereas for the second case first an L(0,1) wave travels on path 1 and then an F(1,1) wave on path 2. Equations (7) and (8) are evaluated for each arrival time t_S of the $i = 1,\ldots,N$ wave packets. Are estimated position from two wave packets within a given tolerance $z_{tol} > 0$, i.e. $|z_{crack,L} - z_{crack,LF}| < z_{tol}$, then the crack location is confirmed at

$$z_{crack} = \frac{z_{crack,L} + z_{crack,LF}}{2} . \tag{9}$$

Absence of a matching reflected flexural wave may be due to several reasons: the measured time is not long enough, the signal threshold θ is too high, or a symmetric discontinuity like a free end that is perpendicular to the propagation direction is present, where no mode conversion occurs.

Thus far, ideal wave excitation and propagation as well as ideal measurement equipment was assumed. In reality however, certain imperfections have to be considered. First, the excitation of the incident wave causes ringing of the actuator, leading to a distorted wave packet even after controlling the excitation [10]. Due to the ringing, the maximum of the wave packet, which is exactly in the middle for an ideal wave, is slightly shifted to a later period. This effect is considered when determining the incident wave's arrival time at the sensor t_{sens} by subtracting a factor of $\alpha_L T$ for $\alpha_L > 0$. Moreover, wave propagation in the considered waveguides is dispersive. Even though dispersion effects for an F(1,1) wave cannot be neglected in the considered frequency range (see Fig. 1), the influence of the distortion of wave packets on the presented algorithm is negligible, i.e. although a flexural wave around 200 kHz is significantly stretched due to dispersion effects, the location of the maximum within the wave remains almost unchanged. Hence, no further adaption of the algorithm is necessary. Last, a static offset t_{off}, caused by delays in measurement equipment, is considered and Eq. (4) is modified to

$$t_S = t_{max} - \frac{n_p}{2} T - t_{off} . \tag{10}$$

Crack Identification

Reflection coefficients $s_{refl,i}$ and transmission coefficients $s_{trans,i}$ describe the ratio of reflected to incident and transmitted to incident wave amplitude, respectively, i.e.

$$s_{refl,i} = \frac{a_{refl,i}}{a_{inc}} \quad \text{and} \quad s_{trans,i} = \frac{a_{trans,i}}{a_{inc}} . \tag{11}$$

Note, $s^2_{\text{refl},i} + s^2_{\text{trans},i} = 1$ holds if no energy is dissipated at the discontinuity. These scattering coefficients can be determined through different numerical methods. If the discontinuity lies in a cross-sectional plane of the waveguide, e.g. for cracks perpendicular to the axial direction, the modal decomposition method can be applied [11]. For more complex crack geometries, a combination of finite element and boundary element techniques is suitable [12]. This technique is not limited to cracks perpendicular to the axial direction and nonzero opening angles can also be analyzed as well as commonly occurring shear cracks. The WFEM is used to describe the mode shapes of propagating and non-propagating modes before and after the cracked area while, in the region of the crack, the Boundary Element Method (BEM) is applied and so the advantages of both methods are combined.

Crack identification is an inverse method, determining the severity of a crack from measurement data. Scattering coefficients, defined in Eq. (11), not only depend on frequency but also on, for example, the crack depth. Hence, if the waves' amplitudes and scattering coefficients are known, the crack depth can be determined through a comparison with simulation data. However, since many parameters affect the scattering coefficients, distinct identification of specific damage properties remains challenging.

EXPERIMENTAL SETUP

In this work, a single wire and a seven-wire cable are studied experimentally. The specimen rests on an insulated solid profile and is fixed using neoprene clamping near both ends. To induce propagating waves, an optimized pulse-signal [10] is generated by a waveform generator and is then amplified by a high-frequency voltage amplifier (peak-to-peak voltage $\sim$250 V). A piezoelectric transducer, which is attached to an end of the specimen, actuates the amplified signal and induces elastic ultrasonic waves in the specimen. Measurements are taken with a Laser Doppler Vibrometer (LDV). Mirrors are used to orient the laser beam perpendicular to the surface of the specimen. The mirrors and the LDV are automatically positioned via a two-axis positioning system. Driving and measurement signals are captured with a high precision oscilloscope and averaging is performed in order to achieve a higher signal-to-noise ratio. All devices are connected to a computer and are remotely configured using a newly developed software environment, allowing for fully automatized experiments. Finally, data analysis is conducted in MATLAB.

RESULTS

Crack Detection in Cylindrical Waveguides

In the following, the proposed crack detection algorithm is applied to a single damaged wire. An artificial crack is sawed into the wire at $z = 1.608$ m, with a crack depth of about 50 % of the wire's diameter.

First, crack detection (level I) and localization (level II) is performed. The normalized LDV output V_{m} of a measurement at $z = 0.81$ m is shown in Fig. 3 in gray, the envelope function V_{env} in black and signal levels above the threshold $\theta = 0.2$ in red. Maxima of the automatically identified wave packets A, B, C and D are marked by $\times$. Note, since amplitudes of reflected L(0,1) waves are comparably low, the threshold has to be chosen appropriately. If transmitted waves are measured, or a piezoelectric sensor is used, θ can be chosen higher to reduce the impact of noise. The algorithm identifies wave packet A as the incident L(0,1) wave. Due to imperfections in wave excitation, a flexural wave packet is also excited, which is wave packet B. The unknown wave packets C and D are identified as reflected L(0,1) and F(1,1) waves, respectively, and the crack location is estimated as $z_{\text{crack}} = 1.620$ m, resulting in an error of less than 1 %. If the delay due to measurement equipment is neglected, the crack is localized at $z_{\text{crack}} = 1.703$ m, which results in an error of about 5.9 %. If distortion of the generated wave packet is neglected as well, the error further increases to 6.7 %, confirming the influence of these two aspects on the precision of the presented algorithm.

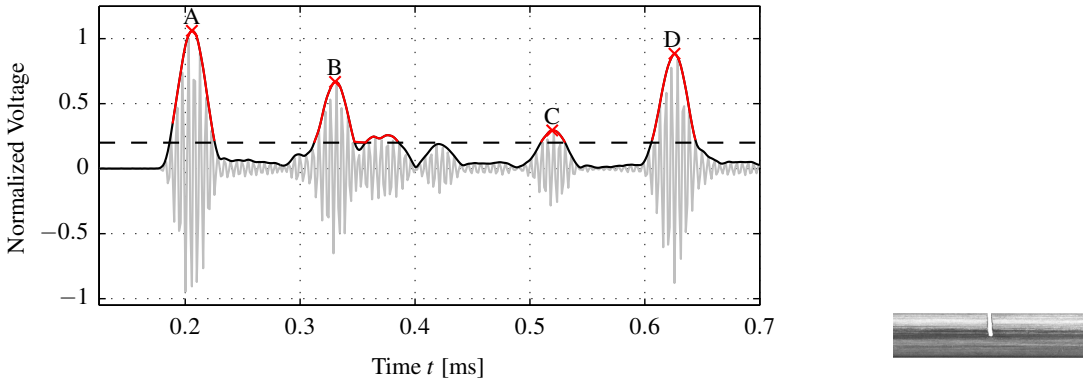


Figure 3: Normalized signal of an LDV measurement at $z = 0.81$ m with threshold $\theta = 0.2$ and identified wave packets. An artificial crack is sawed into the wire at $z = 1.608$ m

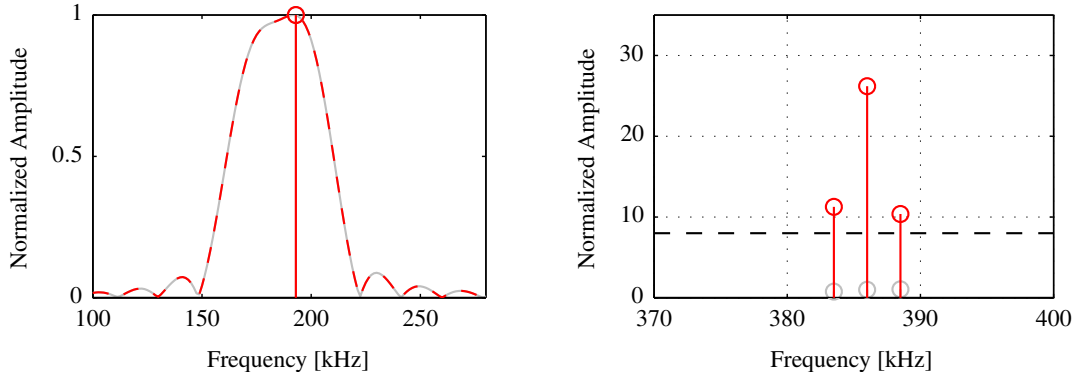


Figure 4: Amplitude of frequency spectrum of a measured signal for an undamaged (gray) and damaged (red) wire around the excitation frequency (left) and second harmonic frequency (right)

As an alternative for accomplishing diagnostic level I, the generation of second harmonic waves is evaluated, as shown in Fig. 4 for the induced wave around 193 kHz. A wave at 386 kHz then only occurs if there is a non-linearity, e.g. due to an increase in the dislocation density [13]. The amplitudes in the frequency spectrum of the induced and second harmonic waves are shown in red for the damaged wire and in gray for an undamaged wire. By defining a threshold, the damaged state can easily be distinguished from the undamaged state. However, since the crack surfaces are clearly separated (sawed crack), and there is no clear increase in the dislocation density, the reason for the occurrence of higher harmonic waves remains unclear.

In a last step, amplitudes of the wave packets are evaluated. Using Eq. (11), the depth of the crack is identified (level III) by comparing the amplitude of the incident wave with the amplitude of the reflected longitudinal wave for a given relation between the scattering coefficient and the crack depth [5]. For the problem at hand, the relevant reflection coefficient is determined by $s_{\mathrm{refl,C}} = \frac{V_{\mathrm{max,C}}}{V_{\mathrm{max,A}}}$, and the crack depth is determined as 46 % of the wire's diameter, which is close to the real crack size.

Crack Detection in Multi-Wire Cables

The proposed crack detection algorithm is also applied to a seven-wire cable. An artificial crack is sawed into the inner wire 7 at $z = 1.90$ m, with a crack depth of about 75 % of the wire's diameter, before the cable is twisted. Waves are excited in wire 1 and an LDV measurement is conducted on the

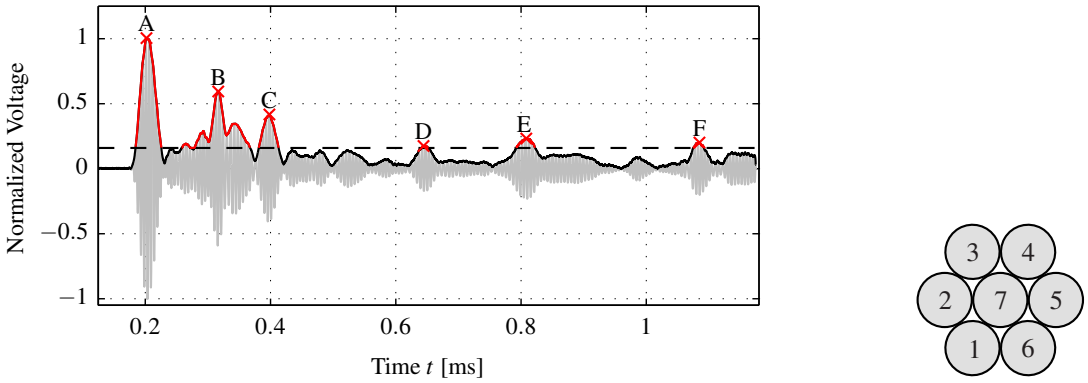


Figure 5: Normalized signal of an LDV measurement at $z = 0.795$ m on wire 1 of a damaged seven-wire cable with highlighted levels above threshold $\theta = 0.16$, and identified wave packets. An artificial crack is sawed into the inner wire 7 at $z = 1.90$ m

same wire at $z = 0.795$ m. In addition to the detection of the crack, crack localization is performed and the normalized LDV signal is shown in Figure 5 in gray, levels above the threshold $\theta = 0.16$ are highlighted and maxima of the wave packets A, B, C, D, E and F are marked by $\times$. The algorithm identifies wave packets A and B as the incident L(0,1) and F(1,1) wave, respectively. Moreover, wave packets D and E are the reflected L(0,1) and reflected F(1,1) wave, and the crack is localized at $z_{\text{crack}} = 1.926$ m with an error of less than 2 %. Hence, even in the case of a seven-wire cable, precise localization of the crack is possible. However, reflected wave packets have very low amplitude since energy of propagating waves transfers to all other wires, and so the threshold has to be chosen accordingly. Also, wave packet C cannot be classified and is therefore considered noise. Wave packet F is the reflected L(0,1) wave from the end of the wire at $z = 3$ m and is also of very low amplitude.

In order to perform crack identification, a further insight into the coupling mechanisms [10] in multi-wire cables is necessary. The direct evaluation of the scattering coefficient $s_{\text{refl,D}} = \frac{V_{\text{max,D}}}{V_{\text{max,A}}}$ leads to an underestimated crack depth of only 35 %. Efficient wave propagation models might be used to improve the results [10].

In addition to previous LDV-based measurements, another measurement is conducted using a piezoelectric sensor to achieve a higher signal-to-noise ratio. The piezoelectric sensor is equivalent to the transducer used as an actuator, and is attached to wire 2 at $z = 0$ m. In contrast to measurements with an LDV, the main axis for this piezoelectric sensor is now in the axial direction. The normalized signal is shown in Fig. 6. Compared to Fig. 5, amplitudes of propagating flexural waves are very low, while propagating longitudinal waves have high amplitudes. Moreover, wave packet B is the reflected L(0,1) wave that is scattered at the crack, and C is the reflected L(0,1) wave from the other end of the wire at $z = 3$ m. While diagnostic levels I and II are easily attainable from this measurement, reaching level III remains challenging due to aforementioned reasons.

Conclusions and Outlook

The proposed crack detection algorithm, which is based on the Hilbert transform, was applied to laboratory experiments on a single damaged wire and a damaged seven-wire cable. It was shown that diagnostic levels I and II are easily achieved by means of this algorithm. For a single wire, also level III is accomplished and the crack depth was successfully identified. Moreover, by considering delays in measurement equipment and ringing of the transducer, the precision of crack localization was significantly improved.

In order to investigate real multi-wire cables, more work still has to be done. Coupling mech-

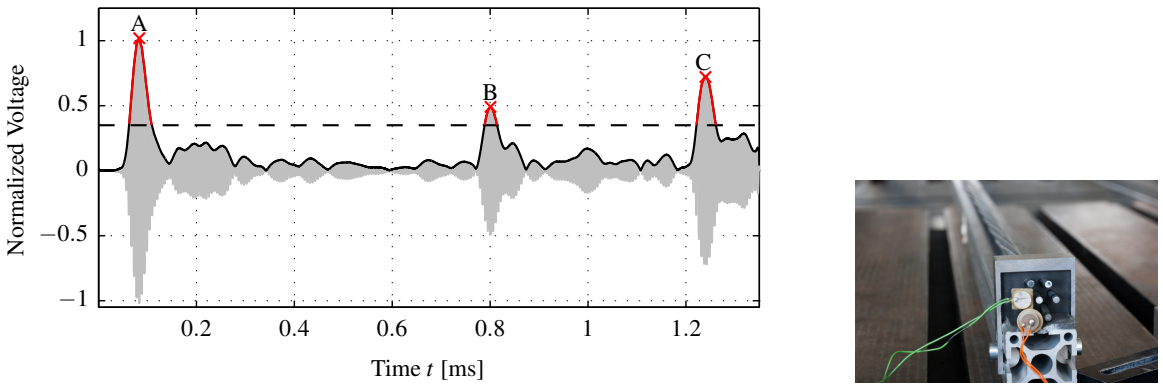


Figure 6: Normalized signal of a piezoelectric measurement at $z = 0\,\mathrm{m}$ on wire 2 of a damaged seven-wire cable with highlighted levels above threshold $\theta = 0.35$, and identified wave packets. An artificial crack is sawed into the inner wire 7 at $z = 1.90\,\mathrm{m}$

anisms of the individual waveguides have to be fully understood, and signal processing has to be improved. Also, more crack characteristics could be identified by using guided ultrasonic waves and a further insight of scattering phenomena. Therefore, further research with FEM and BEM simulations should be conducted in future work.

REFERENCES

[1] M. Biezma and F. Schanack. Collapse of steel bridges. *Journal of Performance of Constructed Facilities*, 21(5):398–405, 2007.

[2] J. Achenbach. *Wave Propagation in Elastic Solids*. North Holland, November 1987.

[3] Daniel Balageas, Claus-Peter Fritzen, and Alfredo Güemes. *Structural health monitoring*. ISTE Ltd, 2006.

[4] Hideo Nishino, Kenichi Yoshida, Hideo Cho, and Mikio Takemoto. Propagation phenomena of wideband guided waves in a bended pipe. *Ultrasonics*, 44, Supplement(0):e1139–e1143, 2006.

[5] Lothar Gaul, Helge Sprenger, Christoph Schaal, and Stefan Bischoff. Structural health monitoring of cylindrical structures using guided ultrasonic waves. *Acta Mechanica*, 223:1669–1680, 2012.

[6] Michel Castaings, Emmanuel Le Clezio, and Bernard Hosten. Modal decomposition method for modeling the interaction of Lamb waves with cracks. *The Journal of the Acoustical Society of America*, 112(6):2567–2582, 2002.

[7] Alexander Pertsch, Jin-Yeon Kim, Yang Wang, and Laurence J Jacobs. An intelligent stand-alone ultrasonic device for monitoring local structural damage: implementation and preliminary experiments. *Smart Materials and Structures*, 20(1):015022, 2011.

[8] B. R. Mace, D. Duhamel, M. J. Brennan, and L. Hinke. Finite element prediction of wave motion in structural waveguides. *The Journal of the Acoustical Society of America*, 117(5):2835–2843, 2005.

[9] Christoph Schaal, Stefan Bischoff, and Lothar Gaul. Analysis of wave propagation in periodic 3D waveguides. *Mechanical Systems and Signal Processing*, 40(2):691–700, 2013.

[10] Christoph Schaal. *Fuzzy Arithmetical Assessment of Health Monitoring for Multi-Wire Cables using Ultrasonic Waves*. Der Andere Verlag, Uelvesbüll, 2014.

[11] Helge Sprenger. *Modeling, Simulation and Experimental Analysis of Ultrasonic Wave Propagation in Cables with Cracked Wires*. Der Andere Verlag, Tönning, 2011.

[12] Stefan Bischoff and Lothar Gaul. Simulation of guided wave interaction with defects in rope structures. In Randall Allemang, James De Clerck, Christopher Niezrecki, and Alfred Wicks, editors, *Special Topics in Structural Dynamics, Volume 6*, Conference Proceedings of the Society for Experimental Mechanics Series, pages 603–609. Springer New York, 2013.

[13] Simon V. Walker, Jin-Yeon Kim, Jianmin Qu, and Laurence J. Jacobs. Fatigue damage evaluation in A36 steel using nonlinear Rayleigh surface waves. *NDT & E International*, 48(0):10–15, 2012.